Electronic Supplementary Material (ESI) for Chemical Science.

Supporting Information

Electrochemical response of surface-attached redox DNA governed by low activation energy electron transfer kinetics

Zhiyong Zheng,[1] Soo Hyeon Kim,[2] Arnaud Chovin,[1] Nicolas Clement,[2,*] and Christophe Demaille [1,*]

[1]Université Paris Cité, CNRS, Laboratoire d'Electrochimie Moléculaire, F-75013 Paris, France

[2]IIS, LIMMS/CNRS-IIS UMI2820, The Univ. of Tokyo; 4-6-1 Komaba, Meguro-ku Tokyo, 153-8505, Japan

Table of Contents

Section 1 – Material and methods

Materials. Doubly HPLC purified, custom functionalized oligonucleotides (oligo-dT), bearing a redox ferrocene (Fc) label at their 3' end and a disulfide group at their 5' extremity, were from Eurogentec (Belgium). Their chemical structure was as shown below:

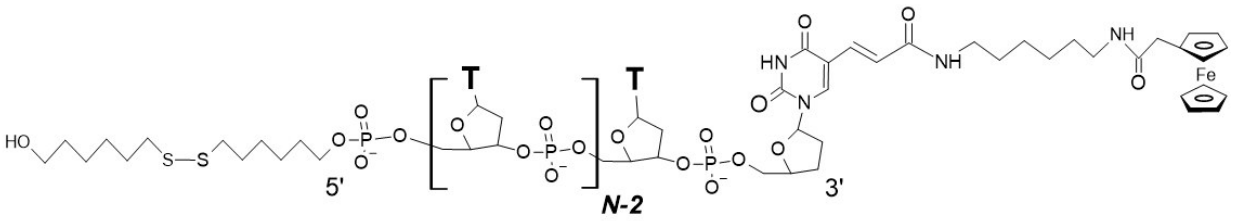

The DNA oligonucleotides were aliquoted in ultrapure water (Millipore) to 100 µM upon arrival and stored at -20 °C in 5 µL aliquots. All other chemicals and solvents were analytical grade and used as received. All reactions were carried out under a wet argon atmosphere, at room temperature, and protected from light.

Preparation of the Fc-dT$_N$ / alkyl thiol solution. The Fc-oligonucleotide-disulfide was reduced to its free thiol form just before grafting. For this, 2 µL of 3.5 mM tris(2-carboxyethyl)phosphine) (TCEP, prepared in 30 mM Tris-HCl buffer, pH 7.5) were added to a 5 µL aliquot of the oligonucleotide, and the reduction was allowed to proceed for 4 h. MCH (6-Mercapto-1-hexanol), released as a by-product of the reduction reaction, was separated from the Fc-oligonucleotide-thiol by using an oligo clean-up and concentration kit (Norgen Biotech). Then, the purified oligonucleotide was recovered in 20 µL. To this volume was added 5 µL of a solution containing either the C_2, C_3, C_4, or C_6 alkyl thiol, prepared in 360 mM PB (88.6 mM NaH_2PO_4, 271.4 mM Na_2HPO_4, pH 7.4) for Fc-dT$_{10}$ and Fc-dT$_{20}$ or 360 mM PBS (88.6 mM NaH_2PO_4, 271.4 mM Na_2HPO_4, 990 mM NaCl, pH 7.4) for Fc-dT$_{35}$ and Fc-dT$_{50}$. The concentration of alkyl thiol was adjusted to ultimately yield the chosen Fc-DNA / alkyl diluent ratio. The final concentration of Fc-DNA in the adsorption solution was 20 µM.

Assembly of Fc-DNA layers. A Teflon mask was used to delimitate a 3 mm diameter disk-shaped region on a freshly exposed template-stripped ultra-flat gold surface (TS-Au).[1] A 20 µL drop of the Fc-DNA/alkyl thiol solution was deposited on this area and the incubation lasted overnight. The drop was replaced several times with 100 mM PB buffer (24.6 mM NaH_2PO_4, 75.4 mM Na_2HPO_4, pH 7.4) to eliminate any weakly grafted Fc-DNA. The surface was subsequently mounted as the bottom of an electrochemical fluid cell. Electrolyte (1 M $NaClO_4$, 10.6 mM NaH_2PO_4, 14.4 mM Na_2HPO_4, pH 7.0) was used to fill to the cell before CV and AFM-SECM characterizations.

Hybridization of surface grafted Fc- dT$_N$. Most of the electrolyte was removed from the cell, leaving a drop of solution on the TS-Au surface. The electrode surface was then covered by a 10 µM complementary oligonucleotide solution (dA$_N$, prepared in the electrolyte), and incubated for 2 h, where after the surface was thoroughly rinsed with electrolyte.

Dehybridization of dsDNA. The surface was thoroughly rinsed with deionized water to dehybridize dsDNA.

CV experiments. CV experiments were performed in a three-electrode configuration with the surface connected as the working electrode. A platinum coil and a KCl-saturated calomel electrode (SCE) served as counter and reference electrodes, respectively. CVs were recorded using a CHI630C electrochemical workstation for scan rates below 200 V/s and a home-built high-bandwidth potentiostat, equipped with positive-feedback ohmic drop compensation, for higher scan rates.[2] Integration of the slow scan rate CVs (0.1 V/s or slower) yielded the molar amount of Fc-DNA chains present on the surface, N_0. Dividing N_0 by the *geometric* surface area of the electrodes, S, yielded the chain coverage, Γ. The inherent smoothness of TS-Au ensures that S is close to the "true" surface

area, as defined at the molecular scale. Hence Γ accurately reflects the actual molecular density of the Fc-DNA layer on the surface.

AFM-SECM characterization. AFM-SECM was carried out using a JPK Nanowizard II microscope combined with a homemade bipotentiostat, in a four-electrode configuration as reported earlier.[3] The Fc-DNA bearing surface was the first working electrode, and a hand-fabricated AFM-SECM tip with a radius of 20 – 50 nm was the second working electrode. A platinum coil and a home-prepared polypyrrole-coated platinum wire (calibrated vs. KCl saturated calomel electrode, SCE) acted as the counter and reference electrodes, respectively. The bipotentiostat allowed us to set independently the potential of the combined AFM-SECM probe and of the TS-Au surface versus the reference electrode, and also to record the tip and gold surface currents.

Section 2 – Supporting figures

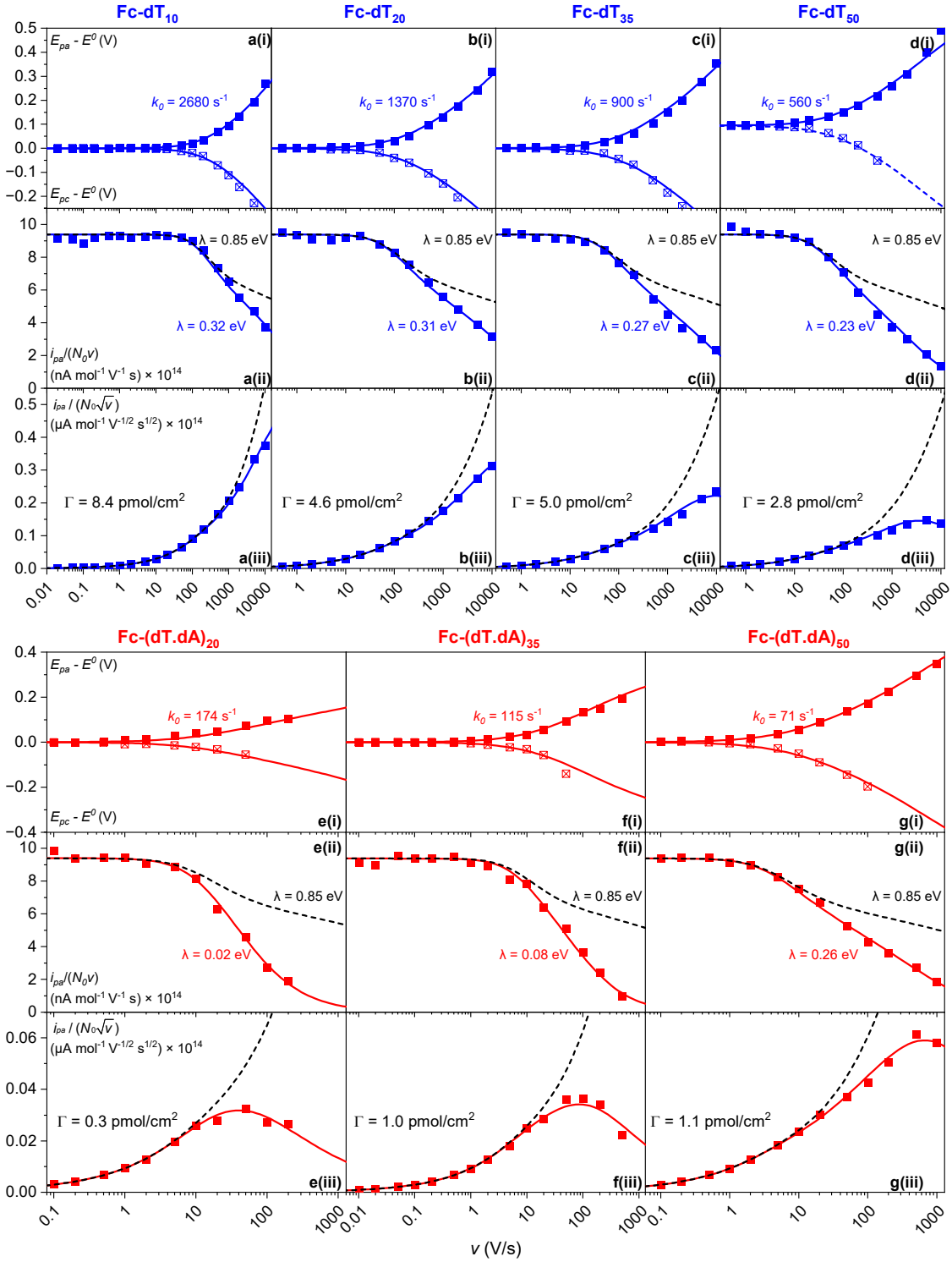

Fig S1. Fc-dT$_N$ and Fc-(dT.dA)$_N$ CV data for various chain lengths (*N* values). Characteristics of the CV signals of electrode end-grafted Fc-dT$_N$ for *N* = 10, 20, 35, and 50 (a, b, c, and d), and Fc-(dT.dA)$_N$ for *N* = 20, 35, and 50 (e, f, and g). Data (symbols) are fitted to the MHL/TLC theoretical curves. Best fit curves and corresponding k_0 and λ values are shown (red and blue traces). The black dashed traces were calculated with the same k_0 values but with λ = 0.85 eV. Phosphate buffered, 1 M $NaClO_4$ aqueous electrolyte, pH = 7. T= 25°C. MCH surface diluent (*n*=6).

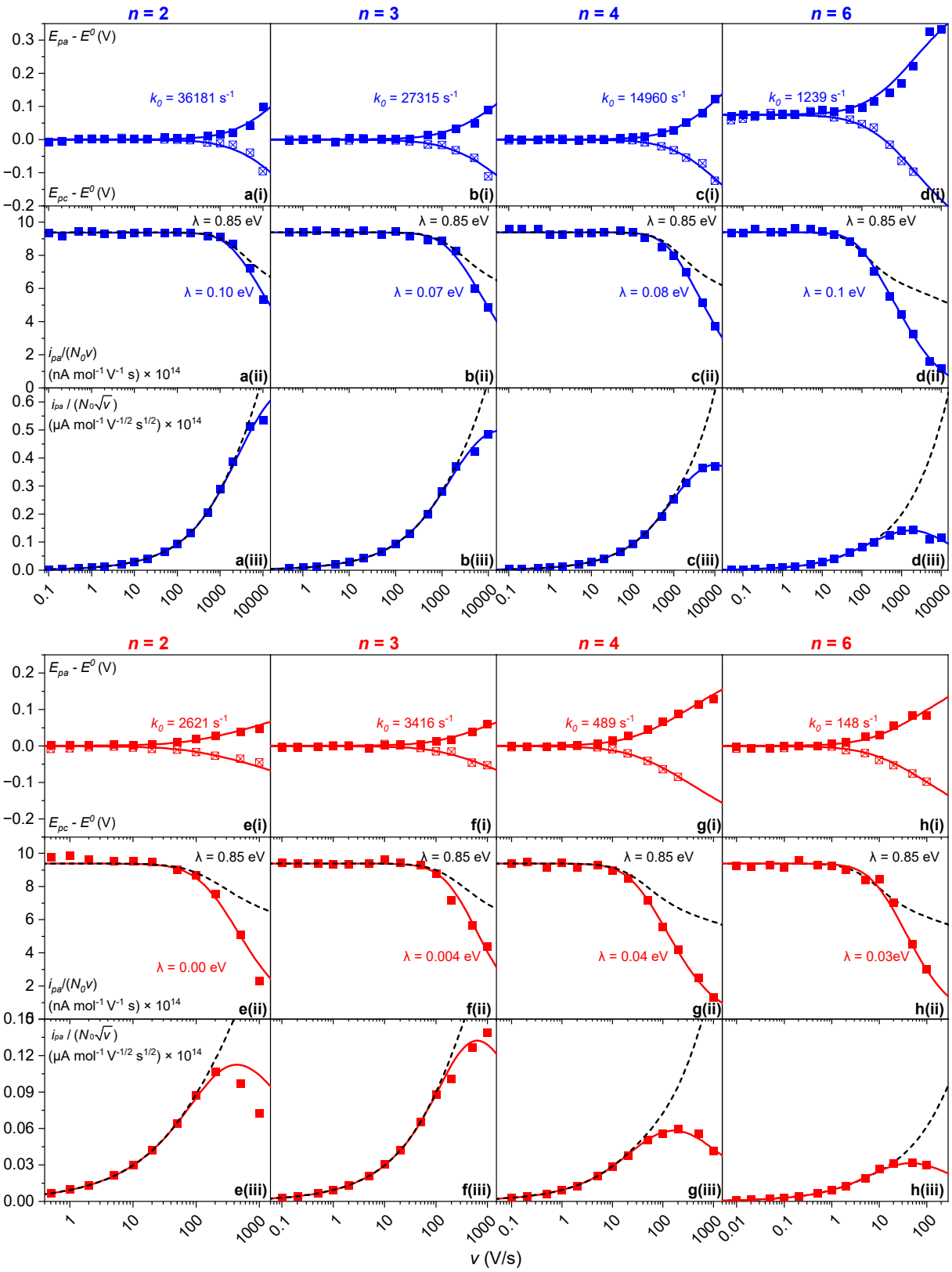

Fig S2. Fc-dT$_{50}$ and Fc-(dT.dA)$_{50}$ CV data for various alkyl diluent chain lengths (*n* values). Characteristics of the CV signals of electrode end-grafted Fc-(dT)$_{50}$ (a, b, c, and d) and Fc-(dT.dA)$_{50}$ (e, f, g, and h) with different alkyl diluent lengths. Data (symbols) are fitted to the MHL/TLC theoretical curves. Best-fit curves and corresponding k_0 and λ values are shown (red and blue traces). The black dashed traces were calculated with the same k_0 values but with λ = 0.85 eV. Phosphate buffered, 1 M $NaClO_4$ aqueous electrolyte, pH = 7. T= 25°C.

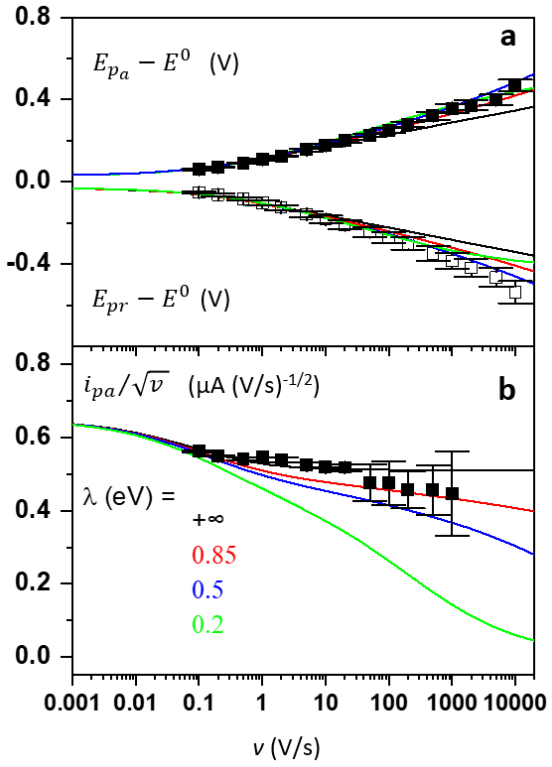

Fig S3. CV measurement of k_s for ferrocene dimethanol at an MCH-coated TS-Au electrode. CV characteristics of 0.2 mM 1,1'-Ferrocenedimethanol (FcdiOH) at a gold TS-electrode modified with a self-assembled monolayer of MCH. (a) Experimental peak potentials and (b) $i_{pa}/\sqrt{\nu}$ ratio are fitted to theoretical curves calculated using the MHL model for a species in solution and for various values of λ, as indicated. Fitting of the peak potential variations yielded a largely λ insensitive best-fit value of $k^d_s = 3 \times 10^{-3}$ cm/s. Fitting the $i_{pa}/\sqrt{\nu}$ data on the working curves did not allow an accurate λ value but showed that, for FcdiOH in solution, λ is larger than 0.5 eV as expected, i.e. much larger than the values we measured herein for Fc-DNA. The error bars in (a) represent a 10 % uncertainty on the determination of the peak potential. The error bars in (b) correspond to uncertainties on the background correction of the diffusive CV (the faradic component varies as $\sqrt{\nu}$ and tends to be lost in the capacitive current at high scan rates). Phosphate buffered, 1 M $NaClO_4$ aqueous electrolyte, pH = 7. T= 25°C.

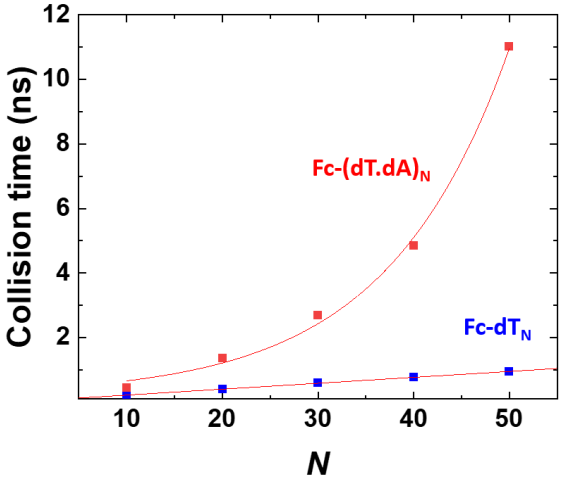

Fig S4. Average collision time of the Fc head with the electrode surface, simulated for single-stranded and hybridized Fc-dT_N chains, for various chain length (*N*) values. Red lines are guides to the eye.

Section 3 – Evidence of the proper terminal self-assembly of Fc-dT layers

It is shown that no chains could be detected on the surface by CV if Fc-dT strands devoid of the thiolated end were used to assemble the layer (Fig S5). We also characterized the structure of the assembled Fc-DNA layer by atomic-force electrochemical microscopy (AFM-SECM). In this technique, a force-sensing microelectrode probe is approached to the surface and used to specifically electrochemically detect the Fc heads of surface-anchored ssDNA chains.[4] As can be seen from Fig S6, Fc heads were detected ~5 to ~15 nm *away* from the anchoring gold surface, at distances correlated to the length (*N*) of the ssDNA strands. The above results are a strong indication that the ssDNA chains were properly anchored via their 5' thiol linker, their 3' Fc-labeled end freely exploring a small volume of solution extending from the surface and solely limited by the chain length.

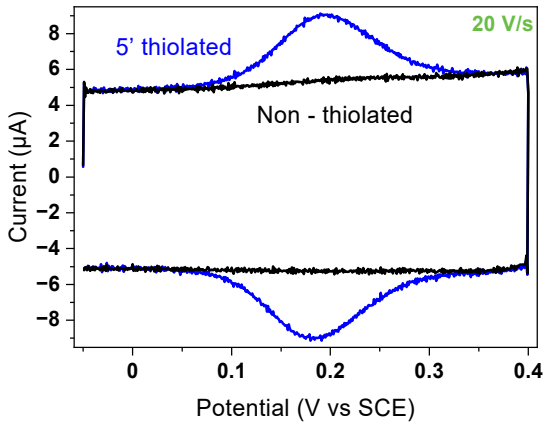

Fig S5. Comparison of CVs recorded at TS-Au electrodes after exposition to 5' thiolated Fc-dT_{20} (blue curve), non-thiolated Fc-dT_{20} (black curve). Phosphate buffered, 1 M $NaClO_4$ aqueous electrolyte, pH = 7. T= 25°C.

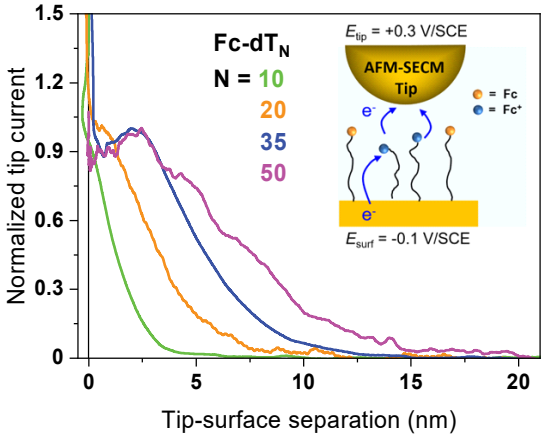

Fig S6. AFM-SECM approach curves recorded at Fc-dT_N layers of various lengths (*N* values), as indicated. The microelectrode-tip current is plotted as a function of the actual tip-substrate distance. Inset: schematics of the tip-to-substrate redox cycling motion of the Fc heads generating the tip current.[4] The tip current is normalized by its peak value. The peak arises from over confinement of the chains. Phosphate buffered, 1 M $NaClO_4$ aqueous electrolyte, pH = 7. T= 25°C.

Section 4 – Numerical calculation of the Fc-DNA CV wave using the MHL/TLC model

The redox Fc head of the DNA chains (both ss and ds) is animated by the fast motional dynamics of the chain. In this thin-layer-cell-like (TLC) situation, the CV response is similar to that of *an immobile* surface-attached redox species, exchanging electrons with the electrode at a rate characterized by the homogeneous standard rate constant k_0. The only difference is that k_0 is modulated by the equilibrium conformational distribution of the chain, which sets the probability of finding the Fc head at the electrode surface. As a result, the CV response of Fc-DNA chains can be calculated using classical equations describing the behavior of a surface-attached species. In the framework of the MHL model, following Savéant's notations,[6] the CV is thus given by the equation:

$$\psi = -\frac{\partial q_0}{\partial \xi} = \Lambda f(\xi)\left[1 - q_0\left(1 + e^{-\xi}\right)\right] \qquad \text{(S1)}$$

Featuring the following dimensionless variables:

- The current, $\Psi = i \,/\, \left(\frac{Fv}{RT} N_0\right)$, with i the actual current, N_0 the molar amount of chains on the electrode, ($N_0 = S\Gamma$ with S the electrode surface area and Γ the chain coverage), and v the potential scan rate.
- The potential, $\xi = \frac{F}{RT}\left(E - E^0\right)$, with E the electrode potential and $E°$ the standard potential of the Fc heads.
- The surface concentration of the species produced at the electrode (Fc^+): $q_0 = \Gamma_{Fc^+}/\Gamma$.
- The parameter $\Lambda = k_0 RT \,/\, (Fv)$, comparing the rate of electron transfer (k_0) to the CV observation time $\tau_{cv} = RT/Fv$.
- $f(\xi)$, a dimensionless function giving the potential dependence of the electron transfer rate as predicted by the MHL model:[6,7]

$$f(\xi) = \int_{-\infty}^{\infty} \frac{exp\left[-\frac{(\lambda^* - \xi - x)^2}{4\lambda^*}\right]}{1 + e^x} dx \Big/ \int_{-\infty}^{\infty} \frac{exp\left[-\frac{(\lambda^* - x)^2}{4\lambda^*}\right]}{1 + e^x} dx$$

where $\lambda^* = \frac{F\lambda}{RT}$ and with λ the reorganization energy (in eV).

Numerically solving Equation S1 for q_0, with the initial condition $q_0 = 0$ at the (negative enough) starting potential of the CV, yields the full $\psi = (\xi)$ CV signal, from which the dimensionless anodic peak current (Ψ_{pa}) and the anodic and cathodic peak potentials (ξ_{pa} and ξ_{pc}) are readily measured.

One can thus obtain working curves representing the CV characteristics as a function of Λ, calculated for a series of λ values, as shown in Fig S7. The plots presented in Fig S7a,b,c are respectively the equivalent of the experimental (E_{pa}, E_{pc}), i_{pa}/v, and $i_{pa}/\sqrt{v}$ versus v plots presented in the main text.

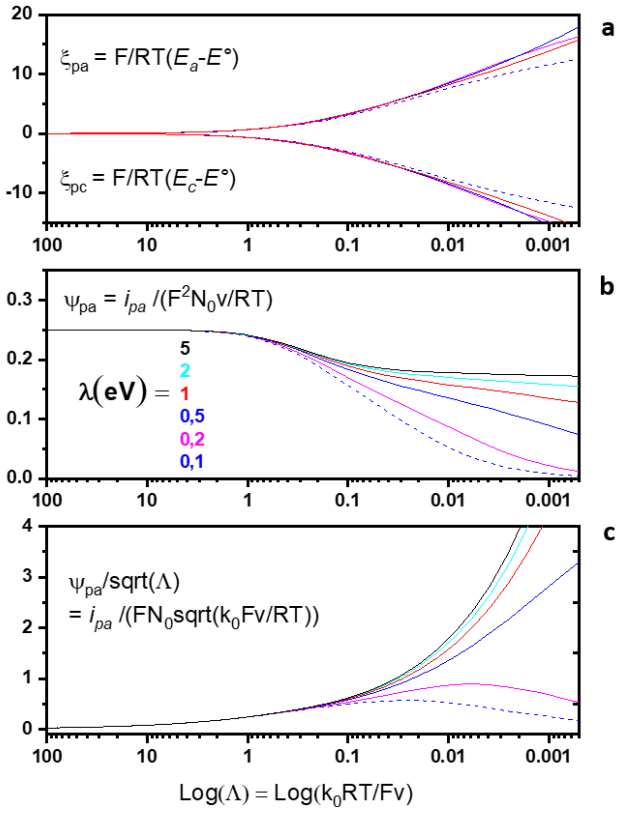

Fig S7. Characteristics of the CV response of a surface-confined redox species obeying MHL electron transfer kinetics. Working curves, calculated with the set of λ values indicated in (b), showing the variation with the parameter Λ of the dimensionless: (a) Forward, ξ_{pa}, and return, ξ_{pc}, peak potentials. (b) Forward peak current, ψ_{pa}. (c) Ratio of ψ_{pa} over $\sqrt{\Lambda}$.

From Fig S7a one can observe the relative insensitivity of the peak positions on the λ value.[8,9] Fig S7c also shows that peak-shaped $i_{pa}/\sqrt{v}$ vs. v curves are only obtained for small enough λ values. More quantitatively, adjusting the experimental (E_{pa}, E_{pc}) v.s. log(v) variation to the theoretical working curves presented in Fig S7a enables the best fit k_0 value to be derived. Using this value, one can then directly superimpose the experimental i_{pa}/v data on the family of theoretical curves presented in Fig S7b. The curve passing closest to the data points indicates the sought λ value. For a more "automated" fitting approach we also implemented equation S1 in python codes which performed a two-parameter fit to derive k_0, λ values. The python code for MHL/TLC fitting is available upon request to the authors. Both approaches yielded comparable values, the automated approach being however faster, more accurate, and providing a standard deviation value (SD) for each of the parameters. The error bars appearing in Figs 4, 5,6 correspond to 3 times the SD value of the individual fits performed to derive k_0 and λ.

Section 5 – Reversibility and specificity of the hybridization of surface attached Fc-dT$_{20}$

Control experiments showed that when the Fc-dT$_{35}$ layer was exposed to a non-complementary dC$_{35}$ strand in solution its CV characteristics remained unchanged (Fig S8). Besides, simple rinsing with deionized water of the electrode exposed to the dA strand restored the CV characteristics of the Fc-dT layers (Fig S9), as expected from the dehybrization of the duplex in low ionic strength solutions.[5]

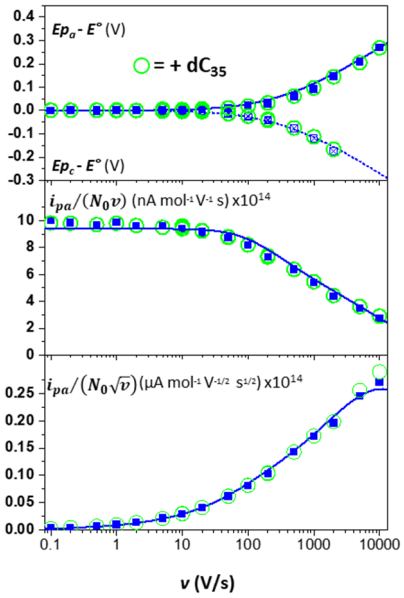

Fig S8. Characteristics of the CV signals of electrode end-grafted Fc-dT$_{35}$ before (blue symbols) and after (open green symbols) exposition to non-complementary dC$_{35}$ in solution. Phosphate buffered, 1 M $NaClO_4$ aqueous electrolyte, pH = 7. T= 25°C.

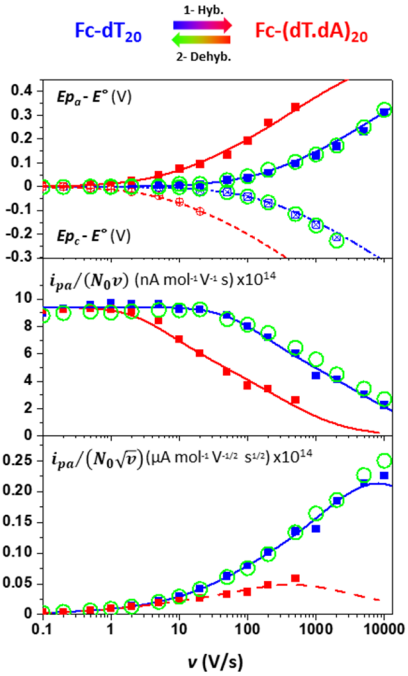

Fig S9. Characteristics of the CV signals of electrode end-grafted Fc-dT$_{20}$ before (blue symbols), after (red symbols) hybridization by fully complementary dA$_{20}$ in solution. Open green circles are data points acquired after de-hybridization of surface-attached Fc-(dT.dA)$_{20}$, carried out by rinsing the electrode with deionized water. Phosphate buffered, 1 M $NaClO_4$ aqueous electrolyte, pH = 7. T= 25°C.

Section 6 – Surface coverage effect on the CV of Fc-$(dT)_{35}$ and Fc-$(dT.dA)_{35}$

We studied systematically the relation between the Fc-DNA coverage on the electrode, Γ, and the CV characteristics. As exemplified in Fig S10, for all of the coverage values explored, the peak potential and peak current variations with scan rate could be very well reproduced using the MHL/TLC model. This yielded sets of k_0, λ values, which are plotted versus the corresponding Γ values in Fig S11, both for Fc-$(dT)_{35}$ and Fc-$(dT.dA)_{35}$ layers.

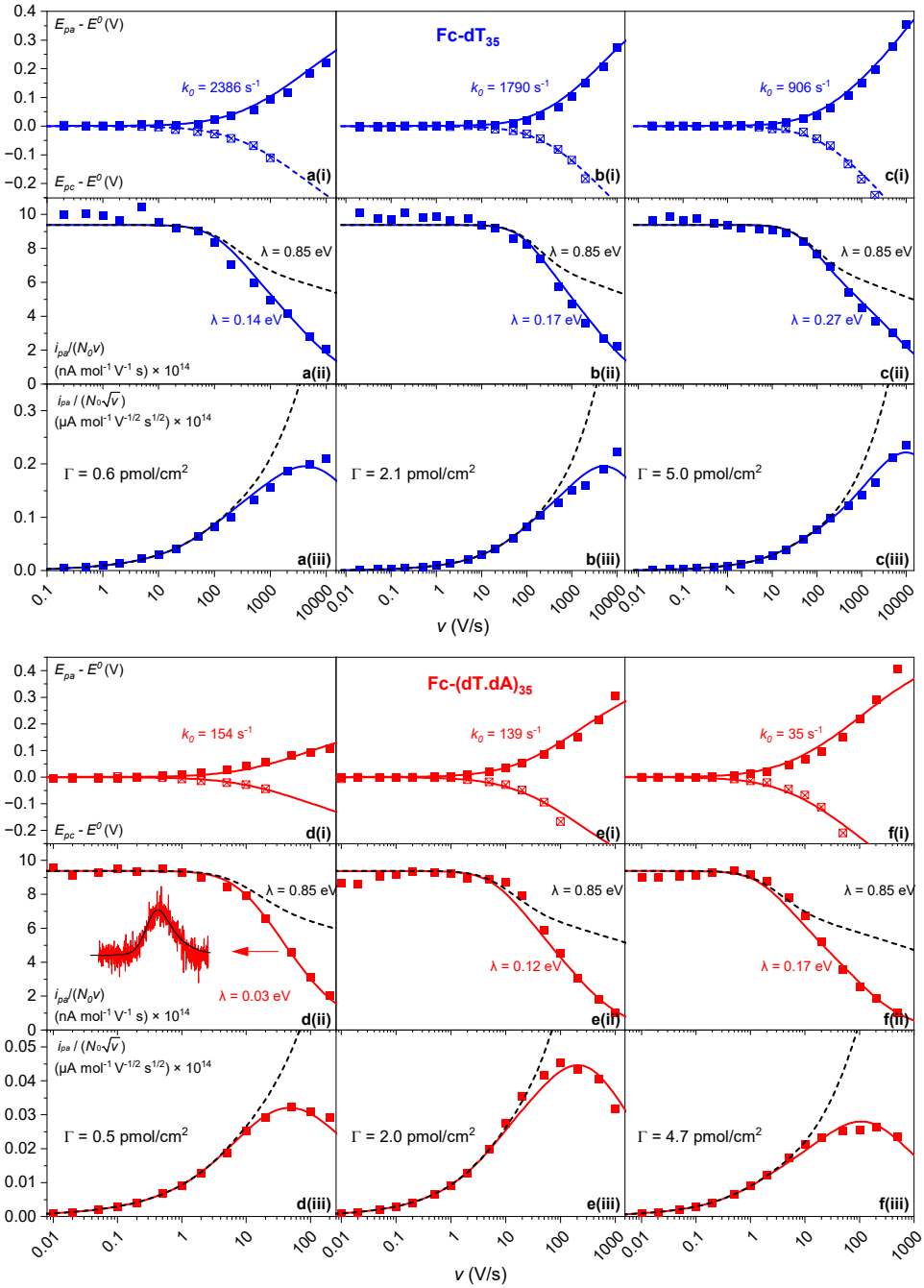

Fig S10. Characteristics of the CV signals of electrode end-grafted Fc-dT_{35} (a, b, and c) and Fc-$(dT.dA)_{35}$ (d, e, and f) with different coverages fitted to the MHL/TLC theoretical curves. Best fit curves and corresponding k_0 and λ values are shown (red and blue traces). The black dashed traces were calculated with the same k_0 values but with λ = 0.85 eV. The inset in d(ii) shows the good adjustment of the experimental (background subtracted, red) and the theoretical (black) anodic CV wave, the latter being calculated with the MHL model for the data point indicated by an arrow. Phosphate buffered, 1 M $NaClO_4$ aqueous electrolyte, pH = 7. T= 25°C. MCH surface diluent (*n*=6).

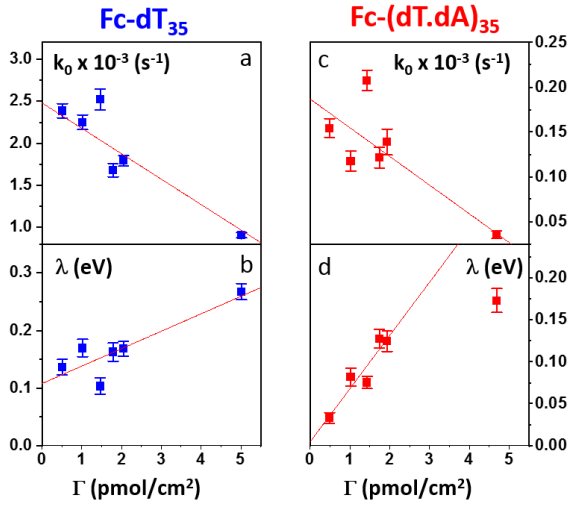

Fig S11. Variation of the kinetic parameters k_0 and λ, characterizing the rate of electron transfer of end-anchored Fc-DNA chains, as a function of the chain coverage Γ. (a,b): Single-stranded Fc-dT$_{35}$. (c,d): Hybridized Fc-(dT.dA)$_{35}$. Red lines are guides to the eye. Error bars correspond to 3 times the standard deviation on the best-fit values for k_0 and λ. Phosphate buffered, 1 M $NaClO_4$ aqueous electrolyte, pH = 7. T = 25°C.

One can observe that, in both cases, k_0 values are the highest for the lowest coverage values and decrease as Γ is increased for N = 35 (Figs 4a and 4c). Conversely, λ values are seen to increase with increasing Γ (Figs 4b and 4d). For Fc-(dT)$_{35}$ layers, λ increases from a lower value of ~0.13 ± 0.03 eV at low coverage, toward 0.25 ± 0.03 eV at the highest coverage. For the Fc-(dT.dA)$_{35}$ duplex, a vanishingly small λ value of ~0.025 eV is recorded at low Γ, and a 0.17 ± 0.03 eV value at the highest coverage.

Lateral interactions between end-grafted chains are expected to become significant when the average distance between the chains' anchoring points on the surface is lower than their length, L_c. Counting 0.7 nm per nucleotide for ssDNA[10] and 0.34 nm for dsDNA,[11] L_c values of 25 nm and 12 nm, can be estimated for Fc-(dT)$_{35}$ and Fc-(dT.dA)$_{35}$, respectively. Hence, interactions can become significant if the coverage greatly exceeds a threshold coverage: $\Gamma_i = 1/(\mathcal{N} L_c^2)$, $\mathcal{N}$ being the Avogadro number. Γ_i is equal to 0.3 pmol/cm^2 for Fc-(dT)$_{35}$ and to 1 pmol/cm^2 for Fc-(dT.dA)$_{35}$. Since the data presented in Fig S11 cover a Γ range of 0.5 to 5 pmol/cm^2 we can conclude that the k_0 and λ vs Γ variations we measured actually translate the modulation of the electron transfer parameters by lateral interactions between neighboring chains. Note that even at the highest Γ value explored (5 pmol/cm^2), the average chain separation is ~6 nm, which is sufficiently large to exclude interactions between *the Fc labels* of neighboring chains, since they are much smaller in size (0.27 nm radius).[12] The k_0 and λ values measured at the lowest coverage value explored (0.5 pmol/cm^2) can reasonably be taken as typical of isolated (non-interacting) chains, whose CV response we primarily intend to model in this work.

Similarly, decreasing k_0 vs. Γ and increasing λ vs. Γ variations were systematically observed for N = 20 and 50 (Fig S12 and Fig S13). These effects translate the modulation of the electron transfer parameters by lateral interactions between neighboring chains. As seen from Fig S11, Fig S12, and Fig S13, the k_0 and λ values measured

at the lowest coverage values explored can be taken as typical of isolated (non-interacting) chains, which we primarily intend to model in this work.

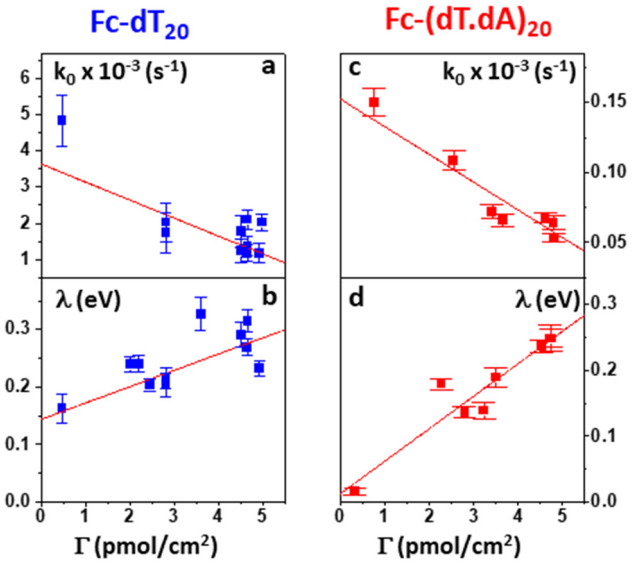

Fig S12. Variation of the kinetic parameters k_0 and λ, characterizing the rate of electron transfer of end-anchored Fc-DNA chains, as a function of the chain coverage, Γ. (a, b): Single-stranded Fc-dT_{20}. (c, d): Hybridized Fc-$(dT.dA)_{20}$. Red lines are guides to the eye. MCH surface diluent (n=6). Phosphate buffered, 1 M $NaClO_4$ aqueous electrolyte, pH = 7. T = 25°C.

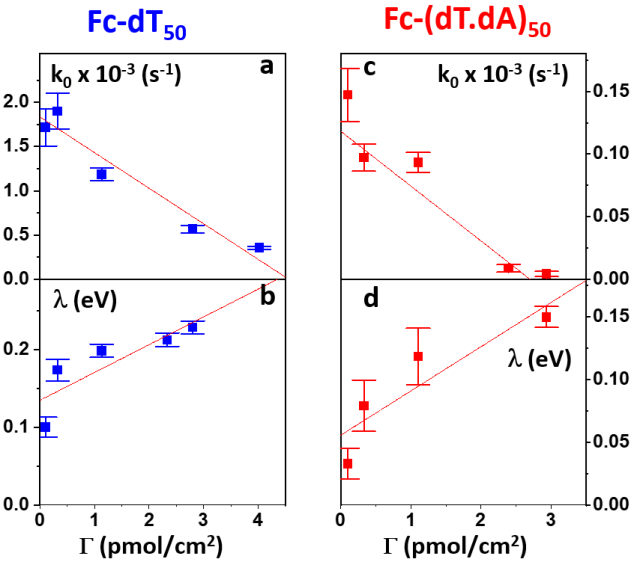

Fig S13. Variation of the kinetic parameters k_0 and λ, characterizing the rate of electron transfer of end-anchored Fc-DNA chains, as a function of the chain coverage, Γ. (a, b): Single-stranded Fc-dT_{50}. (c, d): Hybridized Fc-$(dT.dA)_{50}$. Red lines are guides to the eye. MCH surface diluent (n=6). Phosphate buffered, 1 M $NaClO_4$ aqueous electrolyte, pH = 7. T = 25°C.

Note that for dT50, the chain interaction threshold coverage is $\Gamma_i = 1/(N\ L_c^2) = 0.14$ pmol/cm^2 for Fc-$(dT)_{50}$ and 0.57 pmol/cm^2 for Fc-$(dT.dA)_{50}$, respectively. Which is close from the lowest coverage of 0.25 pmol/cm^2 considered here. Besides the k_0 and λ values measured at this coverage are close to the values that can be extrapolated for Γ=0, ensuring that they correspond to minimal chain interactions.

Section 7 – Molecular dynamics simulations (Qbiol)

Coarse-grained model at the nucleotide level using OxDNA, and post-processing

OxDNA is a nucleotide-level coarse-grained model of DNA[13–16] where each nucleotide is a rigid body that has sites representing the backbone and base (Fig S14). The inter-nucleotide interactions include base stacking, hydrogen bonding between complementary base pairs, a backbone potential, excluded volume, electrostatic interactions between the charged backbones and base, and cross-stacking between diagonally opposite bases in dsDNA. These have been parametrized to reproduce DNA structure, the thermodynamics of hybridization, and the mechanical properties of double and single-stranded DNA. The electrostatic potential is of a Debye-Huckel form and has been fitted to reproduce the [Na^+] dependence of hybridization thermodynamics.[13] We use the full and last version of the model, where the strengths of the stacking and hydrogen-bond interactions do depend on the identity of the base.

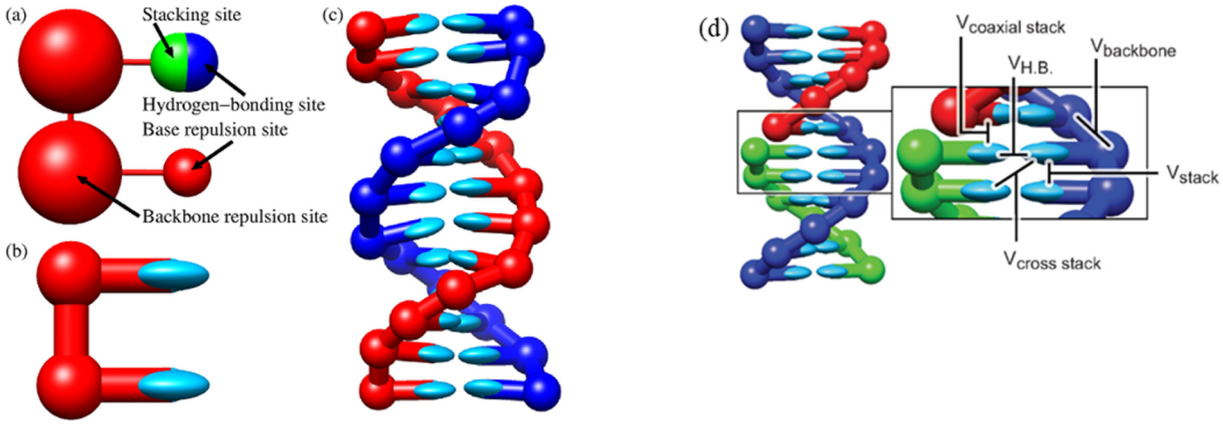

Fig S14. (a) (a) Model interaction sites with their interaction ranges (the typical range is twice the radius of the sphere shown). (b) Representation of these sites in a visualization that makes the planarity of the base clear. (c) A duplex in this representation. Model details, that include these figures, can be found on OxDNA website.[17] (d) Indication of the interactions which hold together a typical duplex.

From a general perspective, coarse-grained models at the nucleotide level have a number of attractive features for considering mechanical properties. They enable sufficiently long simulation times (10 µs in this study). More precisely for MD simulations based on the OxDNA model, the key parameters are:

- At the plates/water boundaries, a very sharp transition with a repulsion plane of a force of 4.863 nN is considered (100 in OxDNA unit).
- The attachment to the surface at the base at the 5' extremity is performed through a punctual trap with an elastic force of 48.63 pN (10 OxDNA units). More specifically, the presence of the thiol monolayer is not considered in Qbiol as it is considered *a posteriori* for rate estimations.
- The base at the 3' extremity is tracked every 909 fs.
- The temperature is set to 20° C.
- A Langevin thermostat was used.

This study is a very specific use of the OxDNA code. Among the technical challenges that had to be overcome, the "DNA grafting" required several steps, starting with a Monte-Carlo simulation, followed by molecular dynamics with progressively increased punctual force until reaching 10 OxDNA units. In addition, as the tracking is performed every 909 fs on a 10 µs time scale, we have developed a python code for direct extraction of the position of the free extremity of DNA and used a RAM disk to avoid errors related to a large quantity of data writing. The Q-biol code also includes data analysis such as $\rho(z)$, βk_c, $\langle \tau_c \rangle$, and slice heat maps as shown in Fig 6. In this study, only a small fraction of the capabilities of Qbiol, needed to discuss the present results of this study, have been presented. A more complete version, that aims to reproduce AFM-SECM results and include electron transfer and counting, will be presented elsewhere. The Qbiol code will be made open to the public.

Supporting references

[1] M. Hegner, P. Wagner, G. Semenza, *Surf. Sci.* **1993**, *291*, 39–46.
[2] A. Anne, C. Demaille, *J. Am. Chem. Soc.* **2008**, *130*, 9812–9823.
[3] L. Nault, C. Taofifenua, A. Anne, A. Chovin, C. Demaille, J. Besong-Ndika, D. Cardinale, N. Carette, T. Michon, J. Walter, *ACS Nano* **2015**, *9*, 4911–4924.
[4] K. Wang, C. Goyer, A. Anne, C. Demaille, *J. Phys. Chem. B* **2007**, *111*, 6051–6058.
[5] D. Kang, X. Zuo, R. Yang, F. Xia, K. W. Plaxco, R. J. White, *Anal. Chem.* **2009**, *81*, 9109–9113.
[6] J.-M. M. Savéant, *J. Phys. Chem. B* **2002**, *106*, 9387–9395.
[7] V. Fourmond, C. Léger, *J. Electroanal. Chem.* **2020**, *879*, 114762.
[8] K. Weber, S. E. Creager, *Anal. Chem.* **1994**, *66*, 3164–3172.
[9] T. M. Nahir, R. A. Clark, E. F. Bowden, *Anal. Chem.* **1994**, *66*, 2595–2598.
[10] Q. Chi, G. Wang, J. Jiang, *Phys. A Stat. Mech. its Appl.* **2013**, *392*, 1072–1079.
[11] R. R. Sinden, in *DNA Struct. Funct.* (Eds.: R.R.B.T.-D.N.A.S. Sinden, Function), Academic Press, San Diego, **1994**, pp. 1–57.
[12] A. M. Bond, R. Colton, J. Harvey, R. S. Hutton, *J. Electroanal. Chem.* **1997**, *426*, 145–155.
[13] "Main Page," can be found under https://dna.physics.ox.ac.uk/index.php/Main_Page.
[14] B. E. K. Snodin, F. Randisi, M. Mosayebi, P. Šulc, J. S. Schreck, F. Romano, T. E. Ouldridge, R. Tsukanov, E. Nir, A. A. Louis, J. P. K. Doye, *J. Chem. Phys.* **2015**, *142*, 234901.
[15] T. E. Ouldridge, A. A. Louis, J. P. K. Doye, *J. Chem. Phys.* **2011**, *134*, 85101.
[16] P. Šulc, F. Romano, T. E. Ouldridge, L. Rovigatti, J. P. K. Doye, A. A. Louis, *J. Chem. Phys.* **2012**, *137*, 135101.
[17] "DNA model introduction," can be found under https://dna.physics.ox.ac.uk/index.php/DNA_model_introduction.